ACS OMEGA

http://pubs.acs.org/journal/acsodf

Article

Identification of a Thyroid Hormone Binding Site in Hsp90 with Implications for Its Interaction with Thyroid Hormone Receptor Beta

Lu Fan, Anusha Kishore, Linda Jansen-Olliges, Dahua Wang, Frank Stahl, Olympia Ekaterini Psathaki, Jennifer Harre, Athanasia Warnecke, Julia Weder, Matthias Preller, and Carsten Zeilinger*

Cite This: *ACS Omega* 2022, 7, 28932−28945

Read Online

ACCESS | Metrics & More | Article Recommendations | Supporting Information

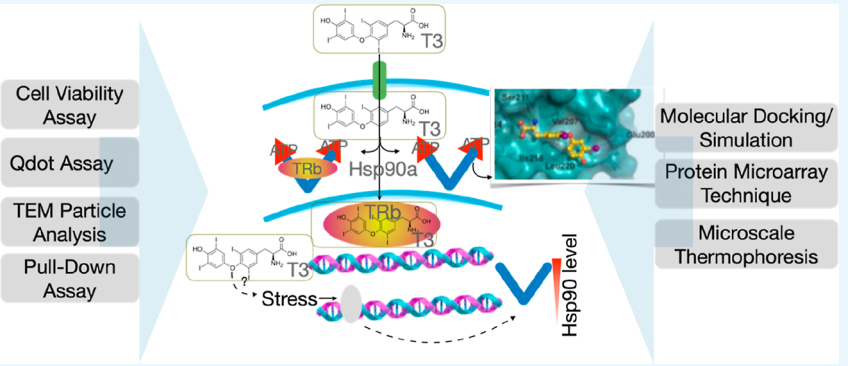

ABSTRACT: While many proteins are known clients of heat shock protein 90 (Hsp90), it is unclear whether the transcription factor, thyroid hormone receptor beta (TRb), interacts with Hsp90 to control hormonal perception and signaling. Higher Hsp90 expression in mouse fibroblasts was elicited by the addition of triiodothyronine (T3). T3 bound to Hsp90 and enhanced adenosine triphosphate (ATP) binding of Hsp90 due to a specific binding site for T3, as identified by molecular docking experiments. The binding of TRb to Hsp90 was prevented by T3 or by the thyroid mimetic sobetirome. Purified recombinant TRb trapped Hsp90 from cell lysate or purified Hsp90 in pull-down experiments. The affinity of Hsp90 for TRb was 124 nM. Furthermore, T3 induced the release of bound TRb from Hsp90, which was shown by streptavidin-conjugated quantum dot (SAv-QD) masking assay. The data indicate that the T3 interaction with TRb and Hsp90 may be an amplifier of the cellular stress response by blocking Hsp90 activity.

INTRODUCTION

Hsp90 is the functional proteome manager as it is required for many newly synthesized proteins and reintroduces damaged proteins into the refolding chaperone cycle.[1−3] Due to its key position and interaction with several hundred cochaperons and client proteins in a cell, it is a target for cancerous cells and a sensitive biomarker for cellular stress.[4−6] Cellular stress occurs when unfolded proteins are formed, for example, by mutations, changes in osmolality, or the redox status. It can be assumed that several steps are required to convert from an unfolded to a folded state. However, some kinases and receptor proteins can also remain in a holding position, waiting for an available chaperone until they are needed and returned to their original function.[7,8] It is known that more than 700 proteins interact with Hsp90, but for some of them, the control points for the reaction are not known.[9,10] A challenge is to observe Hsp90 and its clients' interaction to understand the influencing factors so that cellular responses toward relevant and reliable signals can be distinguished.[2] Hsp90 is a biomarker for cellular stress, whereas the role and function of hormones such as L-tyroxine (T4) and triiodothyronine (T3) and their receptors under stress are unclear, and contradictory results have often been reported depending on the cell type and organism. T4 enhanced thermotolerance in yeast. Nonionizing radiation, such as WiFi connection, may modify the morphology and expression of genes that encode heat shock proteins (Hsp) in the thyroid gland, or the two different thyroid hormone receptor (TR) types can act as oncogenes or as tumor suppressor genes in human cancer.[11−15] Furthermore, the thyroid hormone protects cardiomyocytes from H_2O_2-induced oxidative stress via the phosphoinositide 3-kinase (PI3K)-protein kinase B (Akt) signaling pathway, whereas hypo-

Received: April 14, 2022
Accepted: July 19, 2022
Published: August 9, 2022

https://doi.org/10.1021/acsomega.2c02331
ACS Omega 2022, 7, 28932−28945

Scheme 1. TRb activity under High Hsp90α Level (Stress)[a]

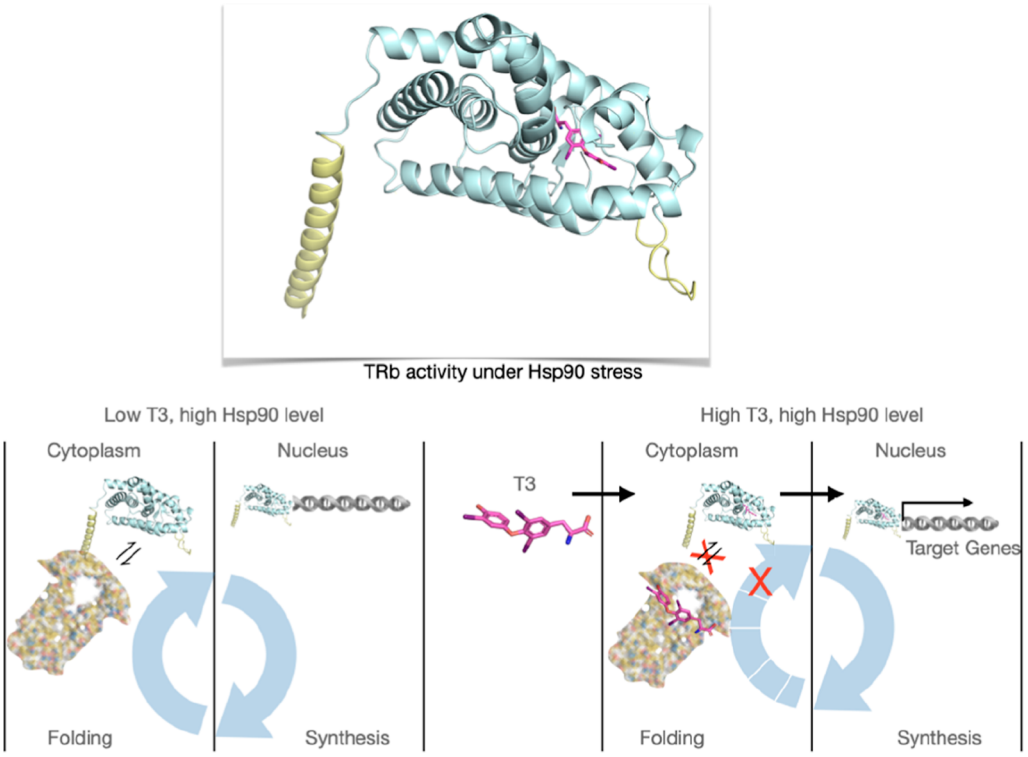

[a]Upper row: cartoon of the TRb (pdb: 3uvv) structure (pale blue) with 3,3′,5 triiodo-L-thyronine (T3, red) in the T3 binding site missing elements added, but incompletely (yellow) modeled by the program AlphaFold. Lower row: putative influence of the low T3 and high Hsp90 level, which induces stress proteins without T3-induced proteins (left). Without T3, a putative interaction between TRb and Hsp90 may occur when the Hsp90 levels increase and TRb is present. Increasing levels of T3 induce the expression of T3-dependent proteins. T3 can influence the TRb-Hsp90 interaction and can bind on TRb and Hsp90 as well.

thyroidism and hyperthyroidism have different effects on heart function.[16,17]

T3 is secreted by the thyroid gland which is regulated by hypothalamus−pituitary−thyroid negative feedback loop.[18,19] T3 is the biological thyroid hormone form compared to its precursor thyronine (T4). Despite that, in the serum is the T4 level 13-fold higher than T3. However, the thyroid gland produces only 20% of the T3 level directly, whereas almost 80% of the T3 level comes from the deiodination of T4.[20,21] T3 binds with a high affinity (pM range) to the thyroid hormone receptor isoforms.[22] It is the natural ligand in the low nanomolar range for thyroid hormone receptor β (TRb) and binds in the receptor's hydrophobic cavity.[23] The thyroid hormone receptors α and β are nuclear receptors and activated by binding thyroid hormones. They are encoded by THRA and THRB genes, which are generated by alternative splicing patterns of primary transcripts, located at the chromosome 17 and 3, respectively.[24,25] The known functional domains of the receptor include a variable N-terminal A/B domain (NTD), a central DNA-binding domain (DBD), a C-terminal ligand-binding domain (LBD), and a linker or joint between the LBD and DBD.[26] TRs are members of the nuclear receptor superfamily, and their functions are tissue- and development-dependent. The beta isoform, TRb, is one of the most attractive members with a wide distribution in organs, and silencing of the TRb gene was also found in aggressive diseases such as malignancies, including thyroid, mammary gland, kidney, liver, and lung cancers.[27−32] The development of the auditory system requires thyroid hormones, and the cochlea is a primary target tissue. Mutations in Slc16a2 and a related gene Slc16a10 (Mct10, Tat1) have recently been shown to cause hearing loss in mice, and deficiency of both transporters is associated with delayed development.[33] Similar to the other nuclear receptors, the transcriptional power of TRb differs based on the cofactor it binds. It binds a corepressor usually in the absence of a ligand, and the transcription is limited, but the corepressor will be cleaved by a coactivator if the ligand is present.[34] The activity of TRb as a transcription factor is fulfilled as a TRE-dependent complex formed by TRb, TRE, and coregulators, which are conditioned by T3 or a TRE-independent pattern, as it was shown that a TRb mutant generated in mice gave a TRE-independent signaling pathway story and TRb bound directly to the PI3K p85 subunit and triggered thereby the upregulation of PI3K-integrin-linked kinase-matrix metalloproteinase-2 signaling path, occurring for both mutant and TRb wild type in the cytoplasm and nucleus.[35]

For other nuclear receptors, such as estrogen or glucocorticoid receptor (GR), the interaction with Hsp90 was clearly confirmed.[10,36−39] Hsp90 inhabits the cytoplasm, with only a minor population existing in the nucleus. In contrast, TRb is located in the nucleus, with a small amount in the cytoplasm, which makes the direct binding of Hsp90 and TRb difficult to detect.[40−45] It is also known that cytoplasmic TRb could exist as a complex with other proteins like MAPK (extranuclear regulated kinase1/2, ERK1/2) in the absence of T3; however, it will shuttle to the nucleus with T3.[46] The impact of T3 on the Hsp90 level as a biomarker of cellular stress is unknown;

https://doi.org/10.1021/acsomega.2c02331
ACS Omega 2022, 7, 28932−28945

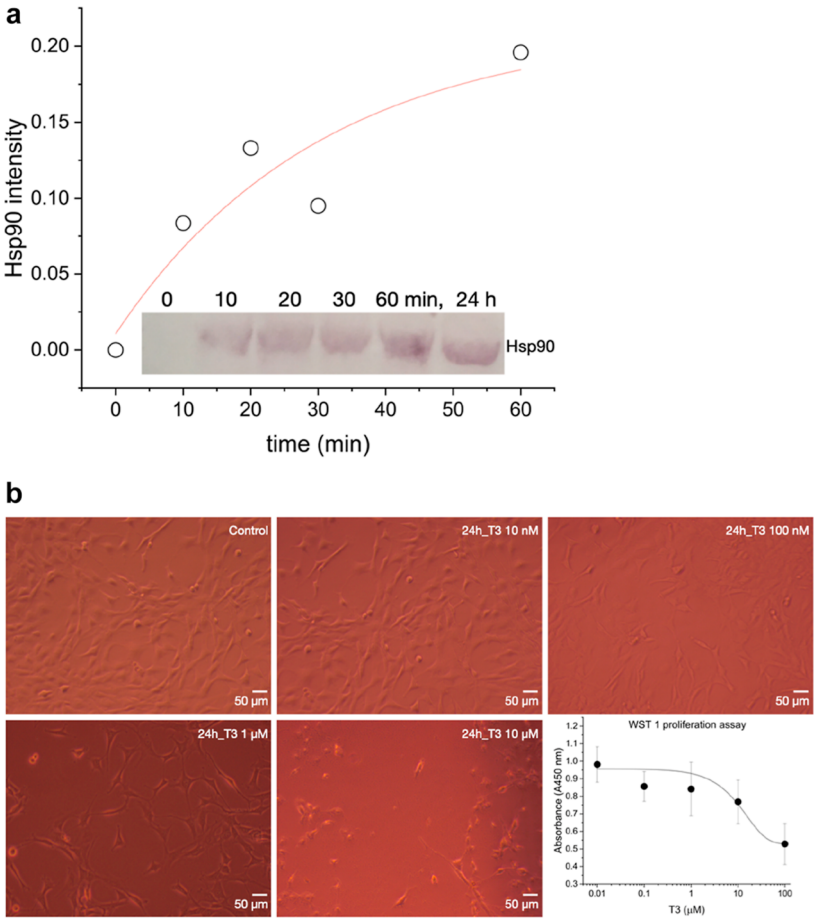

Figure 1. Monitoring of Hsp90 expression in the mouse fibroblast cell line. (a) Immune-blotted cell lysates obtained from the mouse fibroblast cell line (NIH3T3) as a function of time by anti Hsp90 (inset: immune detection of Hsp90). (b) Influence of T3 on the viability of NIH3T3 cells. Microscopy images of cells treated with increasing concentrations of T3 (0−10 μM) and the graph of WST1 assay (T3: 0−100 μM) analyzing the value of mean and standard deviation.

therefore, one assumption could be that TRb interacts with Hsp90 as a stress compensative reaction, but with an increased level of T3, TRb might be released from Hsp90 (Scheme 1).

First, we studied the response of Hsp90 to T3 in fibroblast cells and then conditions that allow the interaction of Hsp90 and TRb. For this purpose, both proteins were synthesized recombinantly. After affinity isolation, the interaction between both proteins was investigated using a recently described highly miniaturized microarray assay technique.[47−49] To study the interaction of T3 or a thyroid mimetic with TRb and Hsp90, different methods were combined, for example, microscale thermophoresis together with a quantum dot-based assay that determines the interaction by quenching the fluorescence intensity.

RESULTS

Influence of Triiodothyronine (T3) on Hsp90. The influence of T3 on Hsp90, corresponding to cellular stress responses, was explored in our study. Therefore, we first examined whether there is a connection in murine fibroblast cell cultures and to what extent T3 can trigger a stress response. For this purpose, murine NIH3T3 fibroblasts treated with and without T3 were disrupted at defined time intervals, and the presence of Hsp90 was analyzed. Without T3, Hsp90 was faintly detected, whereas the addition of T3 (10 μM) resulted in a strong Hsp90 response (Figure 1a, inset). Most of the Hsp90 responses detected by the immunoblot was visible within 10 min, and saturation kinetics followed (Figure 1a). The presence of low and high T3 concentrations strongly influenced the viability of mouse NIH3T3 fibroblasts. After 24 h of cultivation with T3, the cells exhibited different responses, showing lower proliferation ability and poor cell shapes with an increase in T3 (Figure 1b).

We recently identified several Hsp90 inhibitory active compounds when bound ATP-Cy5 was displaced from the ATP-binding pocket of Hsp90 by microarray-based compound screening experiments on Hsp90 (Figure 2a).[40−42] Interestingly, T3 enhanced ATP-Cy5 binding to human Hsp90, but not to the bacterial heat shock protein XcHtpG,[48] while T3 alone gave no fluorescent signal at the same excitation wavelength (Figure 2b). The heat-map showed that the fluorescence intensity was increased with high T3 concentrations, whereas 1 μM radicicol, an Hsp90 inhibitor, displaced bound ATP-Cy5 from both the heat shock proteins. In contrast, T3 enhanced the ATP-Cy5 binding in a dose-responsive manner with a half-maximal effective concentration (EC_{50}) value of 26 nM (Figures 2c and S1). This indicates that ATP-Cy5 was trapped in the ATP binding pocket or that T3 enhanced ATP binding to Hsp90. The comparison of human Hsp90 and bacterial HtpG reveals that the main differences exist in the N-terminal lid domain and a linker domain which occur only in human Hsp90.

https://doi.org/10.1021/acsomega.2c02331
ACS Omega 2022, 7, 28932−28945

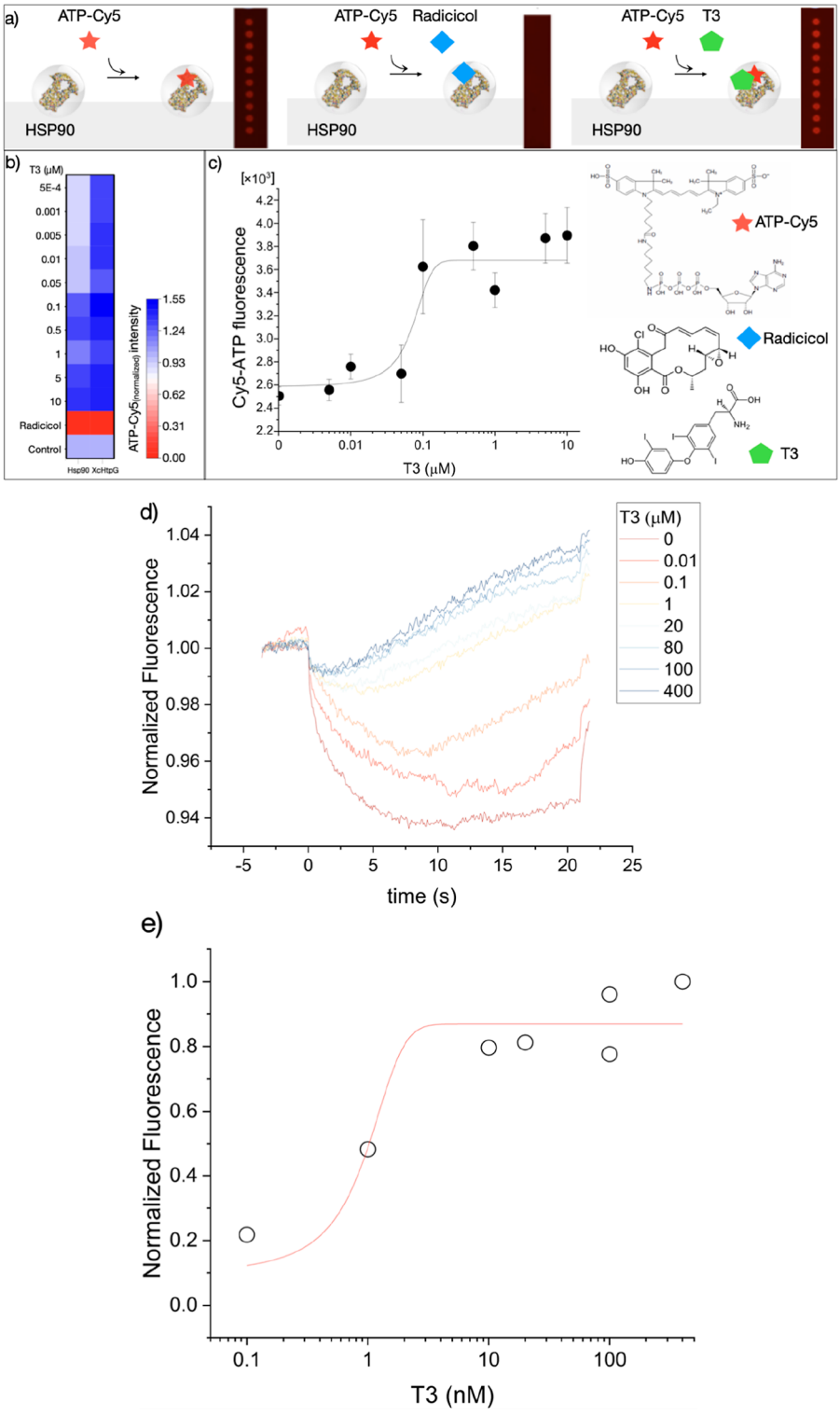

Figure 2. Influence of T3 on binding activity of ATP-Cy5 to Hsp90. (a) Scheme of microarray-based binding assay of ATP-Cy5 on spotted Hsp90 and ATP-Cy5 (left) in the presence of radicicol (middle) or T3 (right) and the corresponding monitoring of the bound ATP-Cy5 at the right side of the microarray. (b) Heat-map of fluorescence intensities obtained from bound ATP-Cy5 to Hsp90 or XcHtpG and (c) corresponding dose-responsive curve of T3 binding to Hsp90. Data are presented as the mean of 10 spots ± S.D. (d) Monitoring of the Hsp90-T3 interaction by MST. MST traces of Cy5-labeled Hsp90 with increasing concentrations of T3 are displayed in the mode of thermophoresis + T-jump. Different concentrations of T3 were indicated by different colored traces. Laser-induced temperature changes for F_{cold} were from −1 to 0 s and F_{hot} from 4 to 5 s applied, respectively. The dose-responsive fittings in (e) were performed with the function $y = A_1 + (A_2 - A_1)/\{1 + 10\hat{}[(\log x_0 - x)*p]\}$ between top and bottom asymptotes, with hill slope p and $\log x_0$ as the center at indicated concentration x.

Additionally, we have estimated the interaction of Hsp90 with T3 by a microscale thermophoresis experiment (MST), running Cy5-labeled Hsp90 and different T3 concentrations. The T3 binding to Hsp90 induced a substantial increase in the

https://doi.org/10.1021/acsomega.2c02331
ACS Omega 2022, 7, 28932−28945

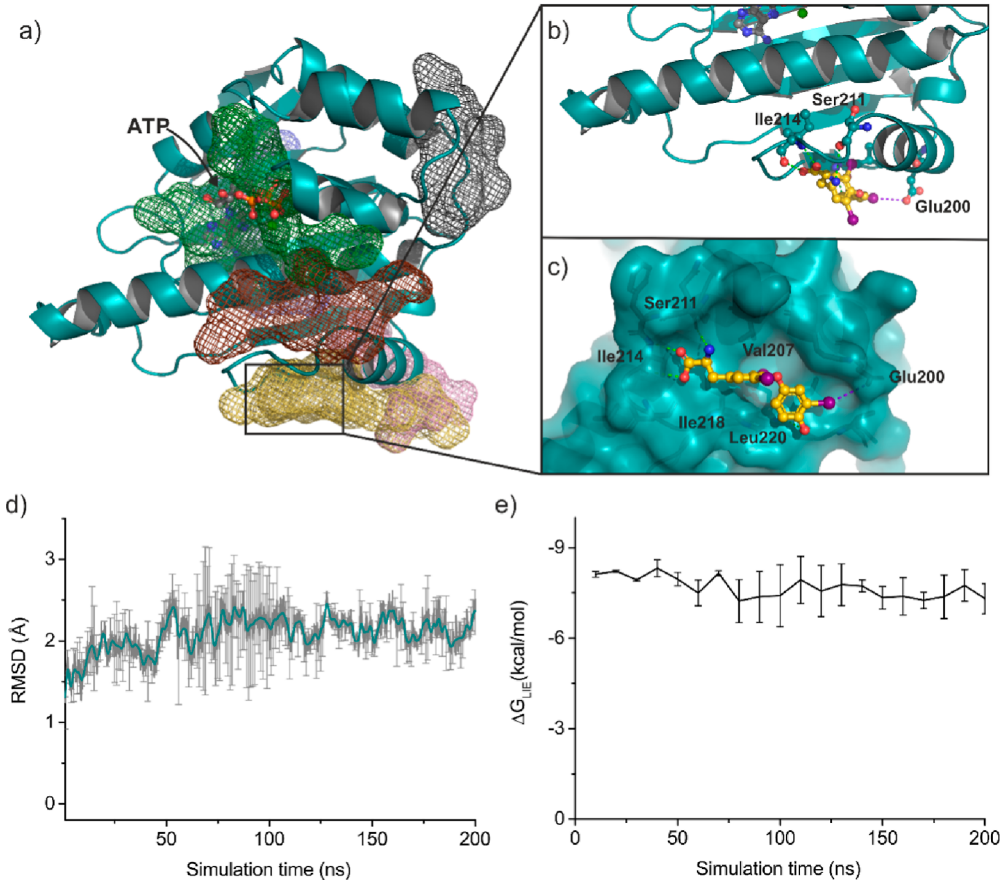

Figure 3. Hsp90 N-terminal domain as the binding target of T3. (a) Overview of the Hsp90 N-terminal domain with the identified binding pockets (colored meshes). (b) Close-up view of the predicted binding position of T3 (yellow) to a pocket, formed by helix 5 and the β8-strand. (c) Interactions of T3 to the residues of the binding pocket. (d) Root mean square deviation (RMSD) of the residues that form the binding pocket along the 200 ns MD simulations (dark cyan line = smoothed data). (e) Interaction energy between T3 and HSP90 along the simulation time, as computed with the LIE method. Data are represented as mean ± SD (n = 2).

fluorescence intensity (Figure 2d,e). Fitting the signal value at the 20th second showed a dose-responsive affinity for Hsp90 with an EC_{50} value of 89 nM. Next, we performed molecular docking experiments to predict the preferred binding site of T3 in Hsp90. First, by constructing affinity maps with AutoLigand[50] for the high-resolution crystal structure of the Hsp90 N-terminal domain with bound ATP (pdb: 3t0z[51]), we identified six possible binding pockets in the structure with different volumes, shapes, and physicochemical properties, including the ATP binding pocket (Figure 3a). Subsequent blind docking allowed us to screen for favorable binding of T3 to the entire Hsp90 crystal structure and confirmed that all these pockets were able to accommodate T3. We finally carried out a series of targeted docking experiments with each of the individual binding pockets as search areas using AutoDock Vina.[52] As a result, we found the most favorable binding position (according to the predicted binding affinity) of T3 in a binding pocket formed by helix 5 (H5) and the β8-strand of the antiparallel β-sheet in the Hsp90 structure (Figure 3b). A total of four hydrogen bonds stabilize the binding of T3 in this position—two hydrogen bonds of the carboxy group of T3 with the backbone atoms of Ile214, one hydrogen bond of the amino group in T3 with the backbone of Ser211, and one hydrogen bond between the hydroxyl group of T3 with the backbone of Leu220—and hydrophobic interactions with residues Val207, Ile218, Leu220, and the CH2 groups of Lys204 (Figure 3c). Additionally, a halogen bond was found between the iodine substituent of the T3 phenol moiety and Glu200. Full atomistic molecular dynamics (MD) simulations of solvated Hsp90 in complex with T3 confirmed that T3 stably binds to the identified binding pocket over the 200 ns simulation time, with only minor fluctuations in the binding pocket (residues 80 and 200−221) (Figure 3d). All MD simulations were performed in duplicates. In addition, we used the linear interaction energy (LIE) method to calculate the binding affinity of T3 to Hsp90. Over the simulation, only marginal differences in the computed binding energy could be observed, and T3 binds with a total binding energy of ΔG_{LIE} = −8.3 ± 0.9 kcal/mol to the identified pocket (Figure 3e).

Is TRb a Client of Hsp90? Nuclear receptors such as estrogen or steroid receptors have been reported to interact with Hsp70 and Hsp90 with and without ligands, in addition to enrichment of other competing proteins and environmental stimuli interfering with the bound complex.[36,53] The STRING software (www.string-db.org) was used to analyze known protein−protein interaction data of Hsp90 and the corresponding putative client proteins. At a low confidence level, no interaction was identified between Hsp90 and TRb. To estimate the conditions for the physical interaction of Hsp90 and TRb and the influence of T3 on both, TRb was recombinantly expressed and purified.[54] First, the TRb gene was cloned into the expression plasmid pETSUMO and hosted

https://doi.org/10.1021/acsomega.2c02331
ACS Omega 2022, 7, 28932−28945

in *Escherichia coli* BL21DE3 cells. Afterward, cell lysates were generated and tested by immunoblotting to detect His-tagged proteins. The expressed proteins gave a band at ∼66 kDa and two additional bands at 130 and 260 kDa (Figure 4a, Lane 1), corresponding to the dimeric and tetrameric forms of TRb. The protein purification required several optimization steps due to some hydrophobic elements in the protein, as a reduced solubility was observed. The purified TRb receptor was visible afterward, the monomer at 66 kDa and the tetramer at 260 kDa (Figure 4a, Lanes 2, 3).

The purified TRb protein was spotted at a concentration of 3 mg/mL onto a microarray, and after blocking, the binding of Hsp90 to TRb was determined via ATP-Cy5 binding to Hsp90 (Figure 4b inset). Titration of Hsp90 resulted in an affinity of 50% for TRb at 124 nM, whereas in the presence of 10 nM T3 or the thyroid mimetic sobetirome, no dose-dependent binding was observed (Figure 4b).

The pull-down experiment with Ni-IMAC-bound TRb confirmed this result, and in the presence of 100 nM T3, no binding of Hsp90 on TRb was observed, whereas, without T3, Hsp90 was bound on purified TRb and eluted after washing, from the Ni-IMAC resin with high imidazole concentration, as shown via anti Hsp90 activity in all fractions by western blot (Figure 4c). This was observed with NIH3T3 cell lysates (Figure 4c, Lanes 1, 2) and with purified Hsp90 (Figure 4c, Lanes 3−7). NIH3T3 cell lysates pretreated without or with T3 were loaded onto a Ni-IMAC resin column charged before with His-tagged TRb. The column was washed with 10-fold washing solution containing 10 mM imidazole and then eluted into a 500 mM imidazole solution. The final elution was then loaded onto SDS-PAGE gel lanes [Figure 4c, Lane 1 (lysate without T3); Lane 2 (lysate with T3)]. Purified Hsp90 was also tested on the column and washed with 10 mM imidazole solution (Figure 4c, Lane 4) and then eluted into a 500 mM imidazole solution (Figure 4c, Lanes 3, 5). Furthermore, Hsp90 was tested in the presence of T3 [Figure 4c, Lane 6 (flowthrough); Lane 7 (final elution)]. This means that the Hsp90 bound TRb on the column in the absence of T3 but do not bound in the presence of T3 in the case of both NIH3T3 lysate and purified Hsp90.

Next, the influence of TRb on the ATP-Cy5 binding of spotted Hsp90 was determined with and without T3. Surprisingly, a quenching effect was observed for the intensity as the TRb concentration increased. Furthermore, we can see ATP displacing the binding of TRb to Hsp90. This finding indicates a 50% displacement activity of TRb at 100 nM, whereas in the presence of 100 nM T3, TRb gave a 12-fold weaker affinity (1.24 μM) for Hsp90 (Figure 4d).

The interaction between Hsp90 and TRb could be visible in tolerable affinities in low concentration ratios so the interaction was investigated by the microarray-based technique. Hsp90 interacts with TRb in the nanomolar range. Therefore, we estimated that the role of T3 in the Hsp90-TRb interaction could be similar to that of glucocorticoid receptors and steroid hormones.[55] To study whether TRb is released from Hsp90 in the presence of the T3 hormone, TRb and Hsp90 were incubated with and without T3, and samples were investigated by SDS-PAGE. Figure 5 shows that after a short incubation for minutes, no difference between samples with and without T3 is observed, whereas after incubation overnight, a clear difference between samples with and without T3 is visible (Figure 5, Lanes 3, 4, 9, 10). Without T3 incubation or after a short incubation, a protein complex was formed at higher molecular

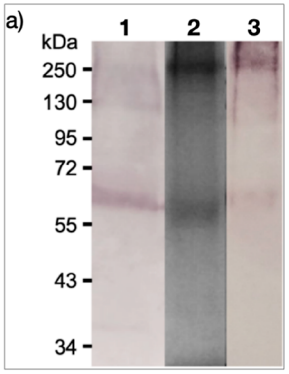

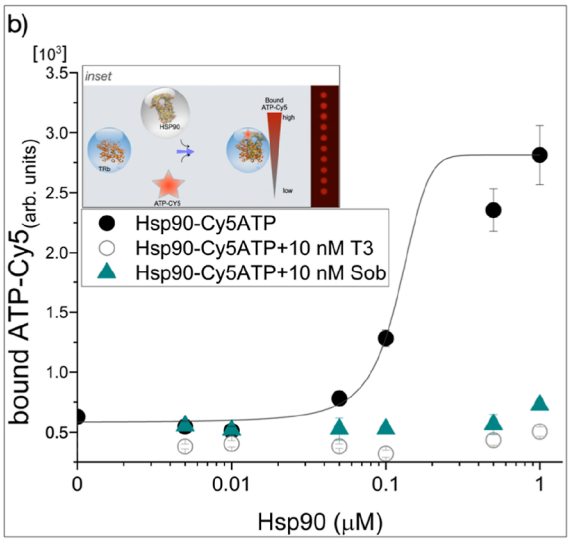

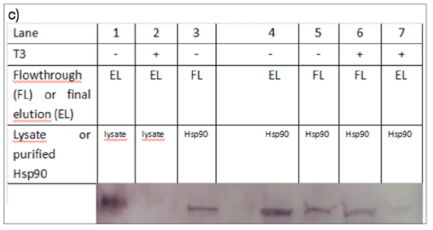

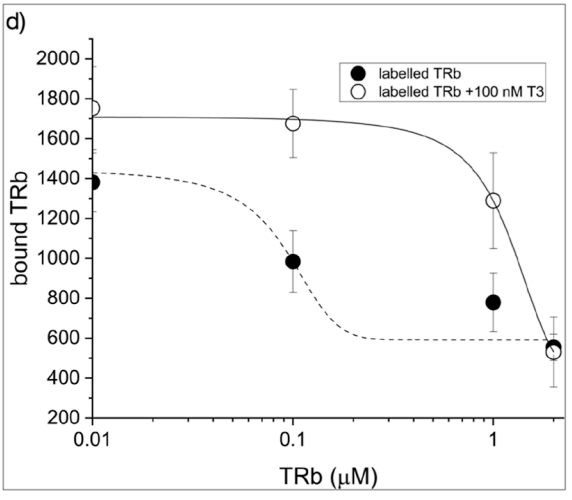

Figure 4. Influence of T3 or sobetirome on the interaction of Hsp90 and spotted TRb. (a) Synthesis and purification of TRb. *E. coli* lysate after expression of TRb (Lane 1) and after Ni-IMAC purification of TRb shown in Coomassie-stained gel (Lane 2) and the corresponding

https://doi.org/10.1021/acsomega.2c02331
ACS Omega 2022, 7, 28932−28945

Figure 4. continued

immunoblot (Lane 3). (b) Inset: microarray-based interaction assay with purified TRb and Hsp90 and Cy5-ATP. (b) Purified TRb was spotted at 3 mg/mL concentration in columns of 10 spots onto the NC microarray. After blocking, each pad was incubated overnight at 4 °C with indicated Hsp90 concentrations and 100 nM ATP-Cy5, whereas it was excluded that the spotted proteins did not bind the fluorescent label. Dose-responsive binding curve of Hsp90 on TRb with and without 10 nM T3 or sobetirome. (c) Immune detection of Hsp90 after elution from bound TRb on the Ni-IMAC resin. Lysates obtained from NIH3T3 cells pretreated for 1 h with or without 100 nM T3 or purified Hsp90 were incubated with TRb bound on the Ni-IMAC resin for 1 h on ice in the absence and presence of T3. The resin was washed with a 10-fold volume of the resin volume, and the bound protein was eluted into buffer containing 500 mM imidazole. The fractions were transferred for SDS-PAGE and immunoblot analysis. The lanes were analyzed by Hsp90 enrichment using anti Hsp90 as the primary antibody with the Lane 1 eluted fraction of NIH3T3 cell lysate without T3 pretreatment, Lane 2 eluted fraction of NIH3T3 cell lysate with T3 pretreatment, Lane 3 eluted fraction of purified Hsp90 without T3 pretreatment, Lane 4 flowthrough of purified Hsp90 without T3 pretreatment, Lane 5 eluted fraction of purified Hsp90 without T3 pretreatment, Lane 6 flowthrough of purified Hsp90 with T3 pretreatment, and Lane 7 eluted fraction of purified Hsp90 with T3 pretreatment. (d) Effect of TRb on Hsp90. The Cy5-ATP intensity of Hsp90 spotted microarray with the increase of TRb without and with T3 of 100 nM. T3-triggered TRb release from Hsp90.

masses of ∼270 kDa [Figure 5, Lanes 1, 2, 6, 7 (short) or 4 overnight]. In the presence of T3 and overnight incubation, the 100 kDa protein band of Hsp90 and the smaller monomeric TRb at ∼70 kDa appeared. However, the immune detection of Hsp90 confirmed that the complex at 270 kDa contained Hsp90 and dissipated in the presence of T3, and more monomeric and less dimeric Hsp90 was visible (Figure 5, Lanes 3, 4, 9, 10). It should be noted that the samples were not heated before loading on the gel.

To estimate the protein binding, SAv-QDs were used to monitor the Hsp90-TRb complex formation as a fluorescence quenching signal (Figure 6a). The advantage of quantum dots on NC microarrays is that the QDs give a high signal intensity and long signal stability with low material consumption of nanolitre volumes. Earlier studies have shown that proteins bound on SAv-QDs quench the fluorescence intensity.[56] First, biotin-ATP was incubated with Hsp90 and bound to SAv-QDs via the biotin-streptavidin interaction, which quenched the fluorescence signal in a dose-responsive manner.[57] Subsequently, the bound Hsp90 was incubated with purified TRb (Figure 6a). Figure 6a shows that the binding of TRb on SAv-QDs charged with biotin-ATP-Hsp90 quenched the fluorescence intensity in a dose-responsive manner which corresponded to the observation of a microarray-based binding assay of Hsp90 and TRb with Cy5-ATP. To investigate whether T3 releases the binding or the bound TRb form, the TRb-Hsp90 complex was incubated with T3. The presence of T3 induced unmasking, and the fluorescence signal of the SAv-QDs was recovered (Figure 6a).

Next, the formation of the TRb-Hsp90 complex was studied by transmission electron microscopy (TEM) analysis using SAv-QDs charged with different combinations of Hsp90 and TRb because quantum dots exhibit a high fluorescence intensity to analyze binding and masking effects. First, SAv-QDs were used here for internal size calibration by TEM. TRb gave a higher density in the presence of the bound proteins with uranyl acetate than those without uranyl acetate. This was measured as the difference in the particle diameter of ∼21 nm and surrounded by the accumulation of the protein material which gave with uranyl acetate an additional ring of ∼10 nm with a higher density (Figure 6b) and showed that the complex was formed.

DISCUSSION

TRb is found in almost all cells and tissues, and the cell physiological setting of T3 is a vulnerable influence that can cause clinical symptoms such as hyperthyroidism or hypothyroidism.[58,59] The physical average plasma total T3 concentration ranges from 1.5 to 3.5 nM, whereas concentrations above and approximately 4.5 nM cause hyperthyroidism.[58] This would mean that high T3 concentrations

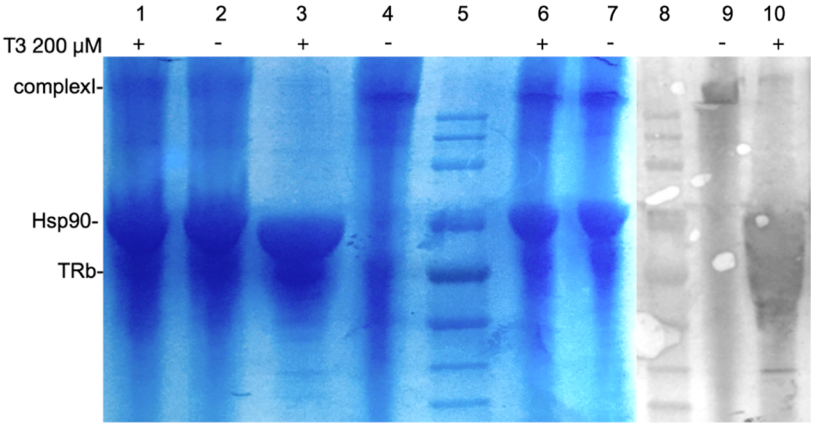

Figure 5. Hsp90-TRb complex formation. Coomassie-stained SDS-PAGE image of the Hsp90-TRb complex with and without T3 after different incubation times with Lanes 1, 3, 6, 10 with 200 μM T3 and Lanes 2, 4, 7, 9 without T3. Samples of Lanes 1, 2 were incubated for 10 min and 6, 7 for 1 h with and without T3 at 4 °C, whereas samples of Lanes 3, 4, 9, 10 were incubated overnight at 4 °C prior to addition of sample buffer and applying onto a precasted gradient gel. Hsp90 and TRb were adjusted to a concentration of 10 μM. Lanes 9 and 10 are the immunoblot of the corresponding Lanes 3 and 4 using the anti Hsp90 antibody. Lanes 5 and 8 correspond to a prestained protein marker with 240 kDa for the largest protein and a red-banded protein for ∼80 and 35 kDa for the smallest protein are shown. Molecular masses were calculated from the linear slope $y = ab^*x$ with −9.09316 ± 0.5109 for the slope and 52.2289 ± 2.54941 for the y cross.

https://doi.org/10.1021/acsomega.2c02331
ACS Omega 2022, 7, 28932−28945

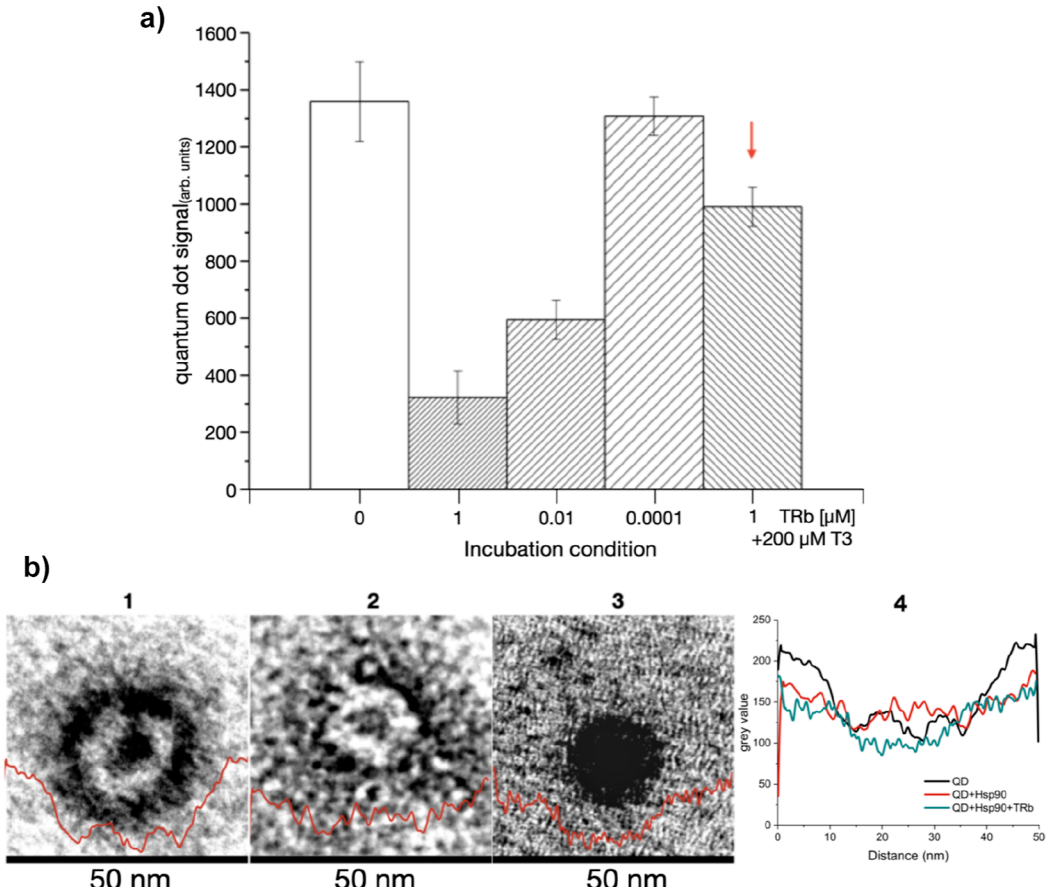

Figure 6. Analysis of the T3-induced release of TRb from Hsp90 by Qdot masking. (a) Masking of the SAv-QD fluorescence by binding Hsp90 and TRb and restoring the SAv-QD fluorescence by 200 μM T3 (red arrow). Incubation conditions without (0) and with TRb in the concentration from 1, 0.01 to 0.0001 μM, and release condition was 1 μM TRb and bound TRb was released with 200 μM T3. All incubations were done overnight at 4 °C. Data are presented as the mean of 10 spots ± S.D. (b) SAv-QDs (1) and charged SAv-QDs with biotin-ATP-Hsp90 (2) or biotin-ATP-Hsp90-TRb complex (3). The particles were stained with 2% uranyl acetate. Comparison of the mean particle diameter by grayscale scans (4). Inset: red lines show grayscale intensity as a function of the enriched contrast material with gray/white color, having a value above 250 and 0 black arbitrary units.

cause two effects on the TRb-Hsp90 interaction, one is the release of TRb, and second is the inhibition of Hsp90 activity by trapping ATP in the binding pocket. If ATP is locked in the ATP binding site, it will lead to cell stress as unfolded protein aggregates are formed, which are toxic to cells.[60,61] We can show that this was a rapid process within 10 min and remained stable up to 24 h or longer because T3 remained stable in the cell culture over such extended periods (Figure 1). To our knowledge, this is a rare observation where T3 directly increases the Hsp90 protein level in vitro corresponding to the role of the stress marker of Hsp90. A direct interaction of T3 at Hsp90 was supported by molecular docking experiments and MD simulation experiments where T3 bound with a total binding energy of $\Delta G_{LIE} = -8.3 \pm 0.9$ kcal/mol to the identified pocket. We showed that T3 or the thyroid mimetic sobetirome released TRb trapped by Hsp90 or hindered Hsp90 binding by microarray-binding assays, pull-down experiments, and complex formation experiments. Using MST measurements with Cy5-labelled Hsp90, we found that T3 bound to Hsp90 in a dose-dependent manner (Figure 2d,e). In addition, the binding of T3 promoted ATP-Cy5 binding to Hsp90 (Figure 2b,c). T3 has a very high affinity for TRb, which had prompted us to apply the concept to our in vitro assays, using highly purified proteins with greater enrichment. High levels of T3 could occur in diseases such as hypothyroidism and put cells under stress by triggering the expression of Hsp90. The docking experiment also confirmed the binding sites of T3 on Hsp90 (Figure 3). Experiments with our microarray assay showed that Hsp90 had bound to TRb, resulting in a modification of the formation, with more ATP being trapped in the ATP pockets of Hsp90 (Figures 4b and 6a). To confirm this protein−protein interaction in the pull-down experiment, purified TRb was incubated with recombinant Hsp90 or Hsp90 lysate, forming the TRb-Hsp90 complex before T3 was presented (Figure 4c). The complex formation was then disrupted by the addition of T3 or sobetirome, both in the microarray showing the release of ATP (Figures 4b and 6a) and in the pull-down column where Hsp90 was released from TRb (Figure 4c). An immunoblot was performed to analyze the complex, which indicated the formation of a complex of Hsp90 and TRb in the absence of T3. However, when incubated overnight with highly concentrated T3, the complex was disrupted, and TRb was released from Hsp90 (Figure 5). The release of TRb affects new transcription processes, while increased cell stress leads to an increase in Hsp90 levels. We suggest that high levels of Hsp90 enable this binding, which indicates that visible binding can only be monitored when higher levels of Hsp90 exist. This may be one

https://doi.org/10.1021/acsomega.2c02331
ACS Omega 2022, 7, 28932−28945

of the reasons why other pull-down experiments gave controversial results with cell-free expression systems.[37,38]

During neuronal development, higher Hsp90 levels occur, and T3 and TRb receptors are relevant for neurogenesis.[62,63] Thyroid hormones have an important function during the human fetal and neonatal developmental periods.[64,65] It was also shown that F-actin polymerization in developing rat brain cells was influenced by T3.[66] This has triggered a debate about possible risks from maternal thyroid disorders, such as hypothyroidism, to the human fetus. There is a need to minimize the risk of mental retardation in the offspring. Given that many individual steps from the synthesis of the hormone to the actual hormonal conversion are susceptible to genetic perturbations and chemicals, these can lead to different thyroid dysfunctions.[65,67] This is also the case when basic building blocks are missing in the diet, as in the case of iodine, or when they are present in the diet, as in the case of thionamides. Furthermore, there is a great deal of evidence showing that various chemicals can alter thyroid function.[68] Additionally, both too low and too high T3 levels can damage the development of the auditory system in the human fetus.[64,65] Interestingly, different degrees of impairments ranging from moderate hearing loss to congenital deafness are accompanied by disturbances of T3 signaling, enabling a time window for treatment in some cases. There is an urgent need for a better understanding of the important role of regulating protein folding in the plasticity of hormonal signals. Here, Hsp90 plays a prominent role in the complete activation of TRb by T3.[37,69] Hsp90 was identified as a biomarker for cell stress and protein maturation and is important for differentiation and development. Our data indicate that the breakdown of the Hsp90-TRb complex elicits the T3 response perhaps in two ways, arresting Hsp90 in the ATP-bound form and releasing TRb, and consequently, the folding machinery is stopped (Scheme 1).

However, many earlier experiments using cell-free expression have shown that TRb lacks the Hsp90 interaction, but Hsp90 has been shown to interact with the glucocorticoid receptor (GR) partially because GR exists in the cytoplasm.[10,37] Our in vitro results indicate a concentration dependency. At physiologically low concentration levels, no interaction is visible, but it occurs with higher stress levels of TRb and Hsp90.[70] This may have consequences for possible background activities arising from T3 surrogates or inhibitors as they appear via environmental exposures.[71]

CONCLUSIONS

Hsp90 is a relevant biomarker for cellular stress.[72−75] In addition, prolonged elevated cell stress via increased Hsp90 levels elicited by T3 could accelerate cell ageing and lead to a continuous reduction of the stem cell reservoir, thus decreasing the regenerative capacity.[15,76,77]

MATERIAL AVAILABILITY

Materials generated in this study are available from the lead contact upon reasonable request.

Data and Code Availability. https://seafile.cloud.uni-hannover.de/smart-link/777c3774-c6b1-4eed-9db1-d79b7abf10d9/.

MATERIALS AND METHODS

Preparation of Human Hsp90a, XcHtpG, and TRb. Hsp90a and XcHtpG were recombinantly synthesized and purified, as described recently.[48] The DNA of TRb was obtained as a codon usage adapted clone from Synbio Technologies LLC, USA, and transferred into the pETSUMO-TA vector plasmid using forward 5′-ATG ACC CCG AAT AGC ATG ACC G-3′ and 5′-TTA CAC TTT ATG CTT CCG GCT C-3́ (Eurofins genomics 3-1414) as reverse primer, respectively, and inserted into the pETSUMO TA cloning plasmid (Figure S2). Afterward, the pETSUMO-TRb construct was transferred into *E. coli* BL21DE3 cells (New England Biolabs C2527H) for the preparation of the recombinant protein. *E. coli* cultures were induced after growing at 37 °C for 8 h by using 0.5 mM IPTG at 14 °C overnight. The cells containing the pETSUMO-TRb construct were sedimented at 8500*g* for 15 min and disrupted in 20 mM Tris, pH 8.0, 137 mM NaCl, 10% (v/v) glycerol, and further lysis of the cells was performed by two cycles in a French cell press, between 14,000 and 16,000 p.s.i. The lysate was adjusted to a final concentration of 8 M urea and 0.5% *N*-lauroylsarcosine and incubated at room temperature for 1 h. The insoluble material was removed by centrifugation at 20,000*g* for 1 h. The TRb protein was supposed to be soluble in the supernatant. Urea and detergent were removed by a PD-10 desalting resin (GE healthcare 17085101), and subsequently, TRb was purified on a Ni-IMAC column (Cube Biotech 74306). Bound His-tagged TRb was incubated with the Ni-IMAC resin at 4 °C overnight in an equilibration buffer of 20 mM Tris, pH 7.5, 50 mM NaCl, 10% (v/v) glycerol, 2 mM β-mercaptoethanol, and 2 mM imidazole and transferred into a column. Afterward, unbound proteins were removed with 10-fold volume of equilibration buffer. Bound proteins were eluted into equilibration buffer containing 250 mM imidazole. The protein concentration was adjusted into a storage buffer containing 20 mM Tris pH 7.5, 50 mM NaCl, 2 mM β-mercaptoethanol, and 10% (v/v) glycerol, using Amicon (30K) centrifugal concentrators (Merck Millipore C7715), to a protein concentration of 3 mg/mL. The presence and purity of TRb were detected by SDS-PAGE and immunoblotting using the mAb anti-His antibody (Epitope Biotech Inc. ABIN559683) and secondary anti-mouse alkaline phosphatase (Sigma-Aldrich A1047).

Detection of Microarray-Based Hsp90 Activity. Purified full-length Hsp90 was transferred into 20 mM Tris−HCl, pH 7.5, 50 mM KCl, 6 mM β-mercaptoethanol, 10% (v/v) glycerol, and spotted on the UniSart 3D nitro slide (Sartorius Stedim Biotech S.A. 2000125). This was done using a contactless GeSim Nano-Plotter (GeSim) with a nanotip pipette at a 3 mg/mL protein concentration and treated before incubation with a blocking solution Cy5-ATP label, as described earlier.[47,48] ATP-Cy5 (Jenabioscience NU-814-CY5) was diluted to a constant concentration of 100 nM in buffer containing 20 mM HEPES-KOH, pH 7.3, 50 mM KCl, 5 mM $MgCl_2$, 20 mM Na_2MoO_4, 0.01% (v/v) Tween 20, 2% (v/v) DMSO, 0.1 mg/mL BSA, and 1 mM DTT. T3 (Cayman Chemical 16028) and sobetirome (AK Scientific, Inc.) were diluted to designed concentrations and added into a black 96-well plate with 100 nM ATP-Cy5. The mixture was then transferred into the chip where 16-well hybridization chambers of Nexterion (Schott, Nexterion) separated the subarrays. After incubation, the slides were washed three times for 5 min with binding buffer. The binding activity of Cy5-labeled ATP was determined by the GenePix 4000B laser scanner (Molecular Devices, Inc.) with 635 nm excitation wavelength, 10% laser power, PMT gain 300, and the activity was then calculated as

https://doi.org/10.1021/acsomega.2c02331
ACS Omega 2022, 7, 28932−28945

values. Evaluation of displacement was done with the EC_{50} value. Furthermore, the evaluation was performed using Origin 8.5G (OriginLab Corporation) to produce fitted graphs.

Fibroblast Cultivation and Immunoblot Analysis. Murine fibroblasts (NIH3T3, ATCC CRL-1658) were cultured in DMEM (Dulbecco's Modified Eagle Medium, Bio&Sell BS.FG 0445) containing 10% FCS (Bio&Sell BS.L 2045) and 1% penicillin−streptomycin-mix (Bio&Sell BS-AB17.07001) at 37 °C in a humidified environment with 5% CO_2. T3 was added into the medium when the cells reached 30−40% confluency. The culture was harvested at the designed time intervals with trypsin (0.02% EDTA included) and then washed with Hank's Buffered Salt Solution (Bio&SELL BS.L 2045). The cell lysates were subsequently generated by adding glass beads and sonicated in buffer (20 mM Tris−HCl, pH 8.0, 500 mM KCl, 2 mM β-mercaptoethanol, 2 mM Imidazole, 10% (v/v) glycerol, 1% protease inhibitor cocktail (Carl Roth 3751.1), 10 mM dithiothreitol) for 10 s and six times on ice. The lysates were centrifugated at a speed of 17,000*g* for 10 min at 4 °C, and the supernatant was analyzed by separation by SDS-PAGE, and immune detection was performed with the anti Hsp90 (StressMarq Biosciences Inc. SMC-147) and anti-mouse alkaline phosphatase secondary antibody (Sigma-Aldrich A1047).

Viability Assay. NIH3T3 cells were split homogeneously into 12-well and 96-well plates at a concentration of 2000 cells/mL in DMEM including 10% FCS and 1% penicillin−streptomycin. T3 was diluted with DMEM complete medium containing 50% DMSO and homogenized into each well at a ratio of 1/1000 when the confluency reached 30−40%, and co-incubated for 24 h at the designed concentrations in both the 12-well plate (T3 varied from 0 to 10 μM) and 96-well plate (T3 varied from 0 to 100 μM). After 24 h of cultivation, the WST-1 reagent (Sigma-Aldrich 11644807001) was diluted at a ratio of 1:10 into each well of the 96-well plate and co-incubated for 1 h. The plates were read at A450nm wavelength, and the data was subsequently analyzed as the viability difference. Scratch assay was performed in a 12-well plate at 30−40% confluency, and cells were cultivated with complete medium containing 10% FCS and 1% penicillin−streptomycin. 50% DMSO was added at a ratio of 1/1000 into the medium as the control. The images of the gap after 24 h culture were captured by an inverted microscope.

Microscale Thermophoresis Analysis. Recombinantly purified human Hsp90a was labeled according to Cy5 mono-reactive dye protein assay (Jenabioscience FP-201-CY5). A pre-run was performed in a MST glass capillary, a proper LED power was checked on Monolith NT.115, and fluorescence between 400 and 700 counts at the final concentration of 50 nM Cy5-labelled Hsp90 was produced. Different combinations of T3 and TRb at constant Hsp90a-Cy5 concentration in buffer containing 20 mM Tris−HCl, pH 7.5, 50 mM KCl, 5 mM β-mercaptoethanol, and 10% (v/v) glycerol were incubated in the dark for 30 min. Then, the samples were transferred into Monolith NT capillaries. The capillaries were inserted into the slots on the sample tray, and the measurements were started with a final constant Hsp90-Cy5 concentration of 50 nM bound with T3 and/or TRb of different concentrations at a LED power of 10%. Data analysis was done by NT analysis software.

Microarray-Based TRb Interaction Array. The purified full-length TRb was transferred into buffer [20 mM Tris−HCl, pH 7.5, 50 mM NaCl, 6 mM β-mercaptoethanol, 10% (v/v) glycerol], spotted at a concentration of 3 mg/mL, blocked, and washed subsequently as described earlier[78] and then incubated at different concentrations of purified full-length human Hsp90a with 100 nM Cy5-labeled ATP (Jena Bioscience NU-814-CY5) in binding buffer [20 mM HEPES-KOH, pH 7.3, 50 mM KCl, 5 mM $MgCl_2$, 20 mM Na_2MoO_4, 0.01% (v/v) Tween 20, 2% (v/v) DMSO, 0.1 mg/mL BSA, 1 mM DTT] for 16 h at 4 °C. Then, the chips were treated as described in part for detection of microarray-based Hsp90 activity. The dose-responsive curves were calculated with Origin 8.5G (OriginLab Corporation) and fitted with the non-linear logistic function, $A_1 = 0$, $A_2 = 1$. Quality validation of the microarray was performed by calculating the mean (S.D.) of 10 spots as described,[47] using a binding buffer with 100 nM dye-labeled ATP.

Pull-Down Assay. Ni-IMAC-bound TRb (100 μL resin) was incubated on ice for 1 h with purified Hsp90 (30 μg) or NIH3T3 cell lysate preincubated with or without T3 (100 nM) on a column. After incubation, the resin was washed with buffer containing 10 mM imidazole, 20 mM Tris, pH 7.5, 50 mM NaCl, 10% (v/v) glycerol, and 2 mM β-mercaptoethanol and eluted with buffer containing 500 mM imidazole, 20 mM Tris, pH 7.5, 50 mM NaCl, 10% (v/v) glycerol, and 2 mM β-Mercaptoethanol. The washing solution and the final elution solution were concentrated to the same concentration. The samples were transferred onto the SDS-PAGE gel, and the presence of Hsp90 was detected after immunoblot analysis.

Streptavidin-Conjugated Quantum Dot-Based Interaction Array. Columns of 10 spots of Sav-QDs (Thermo Q10121MP) were spotted as mentioned in the TRb microarray assay, using the Gesim Nano-Plotter. 50 μL of Biotin-ATP (Jenabioscience NU-277) of different concentrations was added to pads with 45 min incubation in ice and on a rotatory shaker. Biotin-ATP was washed away, and the slide was dried with compressed air. Then, overnight incubation with purified human Hsp90 (3 mg/mL) was done at indicated different concentrations at 4 °C on a rotatory shaker and lastly dried with compressed air. Signal masking of the bound Hsp90 intensity was performed with different TRb concentrations as indicated in the incubation buffer. Masked fluorescence intensity was measured.

Transmission Electron Microscopy. Charged or uncharged Sav-QDs (100 nM) were applied onto negatively glow-discharged carbon-coated 400 mesh copper grids for 1 min, washed twice with distilled water, and stained for 4 min with 2% uranyl acetate. Digital images were collected using the JEM2100Plus (JEOL, Japan) TEM operated at 200 kV equipped with the XAROSA CMOS 20 megapixel camera (EMSIS GmbH, Germany).

Molecular Docking. All docking experiments were carried out with the crystal structure of the Hsp90 N-terminal domain with bound ATP (pdb: 3t0z). The structure of T3 was obtained from the pdb databank. The protein and ligand structures were prepared using AutoDocktools.[79] Blind and targeted docking for each individual pocket in the Hsp90 structure was performed with Autodock Vina,[52] and exhaustiveness and[56] identification of potential binding pockets in the Hsp90 structure was done using AutoLigand.[50]

Molecular Dynamics Simulations and Interaction Energy Calculation. The crystal structure of the human Hsp90 N-terminal domain (pdb: 3t0z) in complex with Mg^{2+} ATP and T3 was fully solvated with the TIP3P water model,[80] and ions were added to obtain a final ion concentration of 0.15

https://doi.org/10.1021/acsomega.2c02331
ACS Omega 2022, 7, 28932−28945

M NaCl. Simulations were performed with NAMD 2.14[81] and the CHARMM36 force field.[82,83] For the parameters of the ligand T3, the CHARMM general force field[84] was used. A minimum distance of 10 Å between the solutes and the water box edges was applied, and all simulations were carried out under periodic boundary conditions. Pressure and temperature were controlled at 1 atm and 310 K by using the Langevin piston method and Langevin dynamics. The cut-off for van-der-Waals interactions and short-range electrostatics was set to 12 Å, and the particle-mesh Ewald method[85] was used for long-range electrostatic interactions. The solvated protein−ligand system was initially energy-minimized and equilibrated. Finally, 200 ns production runs were performed for each system. All MD simulations were performed in duplicates.

The interaction energy between Hsp90 and T3 was computed with the LIE method.[86] The interaction energy ΔG_{LIE} was calculated through the electrostatic (el) and van-der-Waals (vdW) energy contributions of the ligand in complex with Hsp90 (bound) or in solution (unbound) along with the simulation.

$$\Delta G_{LIE} = \alpha(\langle V^{vdW}\rangle_{bound} - \langle V^{vdW}\rangle_{unbound}) + \beta(\langle V^{el}\rangle_{bound} - \langle V^{el}\rangle_{unbound})$$

We used the scaling factors α = 0.18 and β = 0.04 for computing the interaction energies.

■ ASSOCIATED CONTENT

Supporting Information

The Supporting Information is available free of charge at https://pubs.acs.org/doi/10.1021/acsomega.2c02331.

Microarray composition and TRb sequence identity (PDF)

■ AUTHOR INFORMATION

Corresponding Author

Carsten Zeilinger − *BMWZ (Zentrum für Biomolekulare Wirkstoffe), Gottfried-Wilhelm-Leibniz University of Hannover, Hannover 30167, Germany;* orcid.org/0000-0002-6560-0977; Email: zeilinger@cell.uni-hannover.de

Authors

Lu Fan − *BMWZ (Zentrum für Biomolekulare Wirkstoffe), Gottfried-Wilhelm-Leibniz University of Hannover, Hannover 30167, Germany; Clinic for Otorhinolaryngology Surgery, Hannover Medical School (MHH), Hannover 30625, Germany*

Anusha Kishore − *BMWZ (Zentrum für Biomolekulare Wirkstoffe), Gottfried-Wilhelm-Leibniz University of Hannover, Hannover 30167, Germany*

Linda Jansen-Olliges − *BMWZ (Zentrum für Biomolekulare Wirkstoffe), Gottfried-Wilhelm-Leibniz University of Hannover, Hannover 30167, Germany*

Dahua Wang − *BMWZ (Zentrum für Biomolekulare Wirkstoffe), Gottfried-Wilhelm-Leibniz University of Hannover, Hannover 30167, Germany; Clinic for Otorhinolaryngology Surgery, Hannover Medical School (MHH), Hannover 30625, Germany*

Frank Stahl − *Institut für Technische Chemie, Gottfried-Wilhelm-Leibniz University of Hannover, Hannover 30167, Germany*

Olympia Ekaterini Psathaki − *Center of Cellular Nanoanalytics, Integrated Bioimaging Facility, University of Osnabrück, Osnabrück 49076, Germany*

Jennifer Harre − *Clinic for Otorhinolaryngology Surgery, Hannover Medical School (MHH), Hannover 30625, Germany*

Athanasia Warnecke − *Clinic for Otorhinolaryngology Surgery, Hannover Medical School (MHH), Hannover 30625, Germany*

Julia Weder − *Institute for Biophysical Chemistry, Hannover Medical School, Hannover 30625, Germany; Institute for Functional Gene Analytics (IFGA), Department of Natural Sciences, University of Applied Sciences Bonn-Rhein-Sieg, Rheinbach 53359, Germany*

Matthias Preller − *Institute for Biophysical Chemistry, Hannover Medical School, Hannover 30625, Germany; Institute for Functional Gene Analytics (IFGA), Department of Natural Sciences, University of Applied Sciences Bonn-Rhein-Sieg, Rheinbach 53359, Germany*

Complete contact information is available at: https://pubs.acs.org/10.1021/acsomega.2c02331

Author Contributions

L.F. recloned TRb and optimized for protein purification, pull-down experiments, performed microarray-based and MST measurements and cell cultivation, A.K. performed Qdot and microarray based measurement and data valuation, AF performed Hsp90 microarray experiments, L.J.-O. performed MST measurement and data evaluation, O.E.P. performed TEM analysis, D.W. and J.H. did fibroblast cultivation and organization, M.P. and J.W. performed molecular docking experiments and molecular dynamics simulations, F.S., J.H., A.W. and C.Z. gave infrastructural support manuscript input, and C.Z. performed data evaluation and designed experimental concepts. All authors were involved in writing the manuscript.

Notes

The authors declare no competing financial interest.
¶C.Z.—lead contact.

■ ACKNOWLEDGMENTS

L.F. and D.W. were financed by CSC201706180024 and CSC202008080018, respectively; A.K. was funded by the Bundesinstitut für Sportwissenschaft (BISP, ZMVI4-070514/20-21) and E.P. by the DFG SFB 944 Z-Project. The DFG FOR Cytolabs also supported consumables, Excellence Cluster Rebirth Innovation-/Synergy Grants Screening of Telomerase Stimulators for Cardiac Regeneration & Repair (CR&R) by Cell Microarrays and the Cluster of Excellence Hearing4All (EXC 2177/1).

■ REFERENCES

(1) Theodoraki, M. A.; Caplan, A. J. Quality control and fate determination of Hsp90 client proteins. *Biochim. Biophys. Acta* **2012**, *1823*, 683−688.

(2) Schopf, F. H.; Biebl, M. M.; Buchner, J. The HSP90 chaperone machinery. *J. Nat. Rev. Mol. Cell Biol.* **2017**, *18*, 345−360.

(3) Radli, M.; Rüdiger, S. G. D. Dancing with the Diva: Hsp90-Client Interactions. *J. Mol. Biol.* **2018**, *430*, 3029−3040.

(4) Prodromou, C. Mechanisms of Hsp90 regulation. *Biochem. J.* **2016**, *473*, 2439−2452.

(5) Yuno, A.; Lee, M. J.; Lee, S.; Tomita, Y.; Rekhtman, D.; Moore, B.; Trepel, J. B. Clinical Evaluation and Biomarker Profiling of Hsp90 Inhibitors. *Methods Mol. Biol.* **2018**, *1709*, 423−441.

(6) Krüger, K.; Reichel, T.; Zeilinger, C. Role of heat shock proteins 70/90 in exercise physiology and exercise immunology and their diagnostic potential in sports. *J. Appl. Physiol.* **2019**, *126*, 916−927.
(7) Echeverría, P. C.; Bernthaler, A.; Dupuis, P.; Mayer, B.; Picard, D. An interaction network predicted from public data as a discovery tool: application to the Hsp90 molecular chaperone machine. *PLoS One* **2011**, *6*, No. e26044.
(8) Verba, K. A.; Wang, R. Y.; Arakawa, A.; Liu, Y.; Shirouzu, M.; Yokoyama, S.; Agard, D. A. Atomic structure of Hsp90-Cdc37-Cdk4 reveals that Hsp90 traps and stabilizes an unfolded kinase. *Science* **2016**, *352*, 1542−1547.
(9) Picard, D.; Khursheed, B.; Garabedian, M. J.; Fortin, M. G.; Lindquist, S.; Yamamoto, K. R. Reduced levels of hsp90 compromise steroid receptor action in vivo. *Nature* **1990**, *348*, 166−168.
(10) Noddings, C. M.; Wang, R. Y.-R.; Agard, D. A. GR chaperone cycle mechanism revealed by cryo-EM: reactivation of GR by the GR:Hsp90:p23 client-maturation complex. **2020**, 2020.09.12.294975.
(11) Papamichael, K.; Delitheos, B.; Mourouzis, I.; Pantos, C.; Tiligada, E. L. l-Thyroxine induces thermotolerance in yeast. *Cell Stress Chaperones* **2019**, *24*, 469−473.
(12) Misa-Agustiño, M. J.; Jorge-Mora, T.; Jorge-Barreiro, F. J.; Suarez-Quintanilla, J.; Moreno-Piquero, E.; Ares-Pena, F. J.; López-Martín, E. Exposure to non-ionizing radiation provokes changes in rat thyroid morphology and expression of HSP-90. *Exp. Biol. Med.* **2015**, *240*, 1123−1135.
(13) González-Sancho, J. M.; García, V.; Bonilla, F.; Muñoz, A. Thyroid hormone receptors/THR genes in human cancer. *Cancer Lett.* **2003**, *192*, 121−132.
(14) Aranda, A.; Martínez-Iglesias, O.; Ruiz-Llorente, L.; García-Carpizo, V.; Zambrano, A. Thyroid receptor: roles in cancer. *Trends Endocrinol. Metab.* **2009**, *20*, 318−324.
(15) Liu, N.; Matsumura, H.; Kato, T.; Ichinose, S.; Takada, A.; Namiki, T.; Asakawa, K.; Morinaga, H.; Mohri, Y.; De Arcangelis, A.; Geroges-Labouesse, E.; Nanba, D.; Nishimura, E. K. Stem cell competition orchestrates skin homeostasis and ageing. *Nature* **2019**, *568*, 344−350.
(16) Zeng, B.; Liu, L.; Liao, X.; Zhang, C.; Ruan, H. Thyroid hormone protects cardiomyocytes from H2O2-induced oxidative stress via the PI3K-AKT signaling pathway. *Exp. Cell Res.* **2019**, *380*, 205−215.
(17) Stamatouli, A.; Bedoya, P.; Yavuz, S. Hypothyroidism: Cardiovascular Endpoints of Thyroid Hormone Replacement. *Front. Endocrinol.* **2020**, *10*, 888.
(18) Pirahanchi, Y.; Toro, F.; Jialal, I. Physiology, Thyroid Stimulating Hormone. *StatPearls [Internet]*; Treasure Island (FL) StatPearls Publishing, 2022. https://www.ncbi.nlm.nih.gov/books/NBK499850/.
(19) Ortiga-Carvalho, T. M.; Chiamolera, M. I.; Pazos-Moura, C. C.; Wondisford, F. E. Hypothalamus-Pituitary-Thyroid Axis. *Compr. Physiol.* **2016**, *6*, 1387−1428.
(20) Kelly, G. S. Peripheral metabolism of thyroid hormones: a review. *Altern. Med. Rev.* **2000**, *5*, 306−333.
(21) Vagenakis, A. G. Pituitary-thyroid interaction: effects of thyroid hormone, non thyroidal illness and various agents on TSH secretion. *Acta Med. Austriaca* **1988**, *15*, 52−56.
(22) Weinberger, C.; Thompson, C. C.; Ong, E. S.; Lebo, R.; Gruol, D. J.; Evans, R. M. The c-erb-A gene encodes a thyroid hormone receptor. *Nature* **1986**, *324*, 641−646.
(23) Sap, J.; Muñoz, A.; Damm, K.; Goldberg, Y.; Ghysdael, J.; Leutz, A.; Beug, H.; Vennström, B. The c-erb-A protein is a high-affinity receptor for thyroid hormone. *Nature* **1986**, *324*, 635−640.
(24) Sandler, B.; Webb, P.; Apriletti, J. W.; Huber, B. R.; Togashi, M.; Lima, S. T.; Juric, S.; Nilsson, S.; Wagner, R.; Fletterick, R. J.; Baxter, J. D. Thyroxine-thyroid hormone receptor interactions. *J. Biol. Chem.* **2004**, *279*, 55801−55808.
(25) Lazcano, I.; Hernández-Puga, G.; Robles, J. P.; Orozco, A. Alternative ligands for thyroid hormone receptors. *Mol. Cell. Endocrinol.* **2019**, *493*, 110448.
(26) Chen, Y.; Young, M. A. Structure of a thyroid hormone receptor DNA-binding domain homodimer bound to an inverted palindrome DNA response element. *Mol. Endocrinol.* **2010**, *24*, 1650−1664.
(27) Kim, W. G.; Cheng, S. Y. Thyroid hormone receptors and cancer. *Biochim. Biophys. Acta* **2013**, *1830*, 3928−3936.
(28) Puzianowska-Kuznicka, M.; Krystyniak, A.; Madej, A.; Cheng, S. Y.; Nauman, J. Functionally impaired TR mutants are present in thyroid papillary cancer. *J. Clin. Endocrinol. Metab.* **2002**, *87*, 1120−1128.
(29) Silva, J. M.; Domínguez, G.; González-Sancho, J. M.; García, J. M.; Silva, J.; García-Andrade, C.; Navarro, A.; Muñoz, A.; Bonilla, F. Expression of thyroid hormone receptor/erbA genes is altered in human breast cancer. *Oncogene* **2002**, *21*, 4307−4316.
(30) Puzianowska-Kuznicka, M.; Nauman, A.; Madej, A.; Tanski, Z.; Cheng, S.; Nauman, J. Expression of thyroid hormone receptors is disturbed in human renal clear cell carcinoma. *Cancer Lett.* **2000**, *155*, 145−152.
(31) Lin, K. H.; Shieh, H. Y.; Chen, S. L.; Hsu, H. C. Expression of mutant thyroid hormone nuclear receptors in human hepatocellular carcinoma cells. *Mol. Carcinog.* **1999**, *26*, 53−61.
(32) Dobrovic, A.; Houle, B.; Belouchi, A.; Bradley, W. E. erbA-related sequence coding for DNA-binding hormone receptor localized to chromosome 3p21-3p25 and deleted in small cell lung carcinoma. *Cancer Res.* **1988**, *48*, 682−685.
(33) Sharlin, D. S.; Ng, L.; Verrey, F.; Visser, T. J.; Liu, Y.; Olszewski, R. T.; Hoa, M.; Heuer, H.; Forrest, D. Deafness and loss of cochlear hair cells in the absence of thyroid hormone transporters Slc16a2 (Mct8) and Slc16a10 (Mct10). *Sci. Rep.* **2018**, *8*, 4403.
(34) Yen, P. M.; Ando, S.; Feng, X.; Liu, Y.; Maruvada, P.; Xia, X. Thyroid hormone action at the cellular, genomic and target gene levels. *Mol. Cell. Endocrinol.* **2006**, *246*, 121−127.
(35) Furuya, F.; Ying, H.; Zhao, L.; Cheng, S. Y. Novel functions of thyroid hormone receptor mutants: beyond nucleus-initiated transcription. *Steroids* **2007**, *72*, 171−179.
(36) Chambraud, B.; Berry, M.; Redeuilh, G.; Chambon, P.; Baulieu, E. E. Several regions of human estrogen receptor are involved in the formation of receptor-heat shock protein 90 complexes. *J. Biol. Chem.* **1990**, *265*, 20686−20691.
(37) Dalman, F. C.; Koenig, R. J.; Perdew, G. H.; Massa, E.; Pratt, W. B. In contrast to the glucocorticoid receptor, the thyroid hormone receptor is translated in the DNA binding state and is not associated with hsp90. *J. Biol. Chem.* **1990**, *265*, 3615−3618.
(38) Baniahmad, A.; Ha, I.; Reinberg, D.; Tsai, S.; Tsai, M. J.; O'Malley, B. W. Interaction of human thyroid hormone receptor beta with transcription factor TFIIB may mediate target gene derepression and activation by thyroid hormone. *Proc. Natl. Acad. Sci. U.S.A.* **1993**, *90*, 8832−8836.
(39) Zhang, J. B.; Roggero, V. R.; Allison, L. A. Nuclear Import and Export of the Thyroid Hormone Receptor. *Vitam. Horm.* **2018**, *106*, 45−66.
(40) Sreedhar, A. S.; Kalmár, E.; Csermely, P.; Shen, Y. F. Hsp90 isoforms: functions, expression and clinical importance. *FEBS Lett.* **2004**, *562*, 11−15.
(41) Daniel, S.; Bradley, G.; Longshaw, V. M.; Söti, C.; Csermely, P.; Blatch, G. L. Nuclear translocation of the phosphoprotein HOP (HSP70/HSP90 organizing protein) occurs under heat shock and its proposed nuclear localization signal is involved in HSP90 binding. *Biochim. Biophys. Acta* **2008**, *1783*, 1003−1014.
(42) Hance, M. W.; Nolan, K. D.; Isaacs, J. S. The double-edged sword: conserved functions of extracellular HSP90 in wound healing and cancer. *Cancers* **2014**, *6*, 1065−1097.
(43) Holownia, A.; Mroz, R. M.; Kielek, A.; Chyczewska, E.; Braszko, J. J. Nuclear HSP90 and HSP70 in COPD patients treated with formoterol or formoterol and corticosteroids. *Eur. J. Med. Res.* **2009**, *14*, 104−107.
(44) Kang, K. I.; Meng, X.; Devin-Leclerc, J.; Bouhouche, I.; Chadli, A.; Cadepond, F.; Baulieu, E. E.; Catelli, M. G. The molecular chaperone HSP90 can negatively regulate the activity of a

https://doi.org/10.1021/acsomega.2c02331
ACS Omega 2022, 7, 28932−28945

glucocorticosteroid-dependent promoter. *Proc. Natl. Acad. Sci. U.S.A.* **1999**, *96*, 1439−1444.
(45) Sawarkar, R.; Paro, R. HSP90@chromatin.nucleus: an emerging hub of a networker. *Trends Cell Biol.* **2013**, *23*, 193−201.
(46) Cao, H. J.; Lin, H. Y.; Luidens, M. K.; Davis, F. B.; Davis, P. J. Cytoplasm-to-nucleus shuttling of thyroid hormone receptor-beta1 (Trbeta1) is directed from a plasma membrane integrin receptor by thyroid hormone. *Endocr. Res.* **2009**, *34*, 31−42.
(47) Schax, E.; Walter, J. G.; Märzhäuser, H.; Stahl, F.; Scheper, T.; Agard, D. A.; Eichner, S.; Kirschning, A.; Zeilinger, C. Microarray-based screening of heat shock protein inhibitors. *J. Biotechnol.* **2014**, *180*, 1−9.
(48) Yue, Q.; Stahl, F.; Plettenburg, O.; Kirschning, A.; Warnecke, A.; Zeilinger, C. The Noncompetitive Effect of Gambogic Acid Displaces Fluorescence-Labeled ATP but Requires ATP for Binding to Hsp90/HtpG. *Biochemistry* **2018**, *57*, 2601−2605.
(49) Hermane, J.; Eichner, S.; Mancuso, L.; Schröder, B.; Sasse, F.; Zeilinger, C.; Kirschning, A. New geldanamycin derivatives with anti Hsp properties by mutasynthesis. *Org. Biomol. Chem.* **2019**, *17*, 5269−5278.
(50) Harris, R.; Olson, A. J.; Goodsell, D. S. Automated prediction of ligand-binding sites in proteins. *Proteins* **2008**, *70*, 1506−1517.
(51) Li, J.; Sun, L.; Xu, C.; Yu, F.; Zhou, H.; Zhao, Y.; Zhang, J.; Cai, J.; Mao, C.; Tang, L.; Xu, Y.; He, J. Structure insights into mechanisms of ATP hydrolysis and the activation of human heat-shock protein 90. *Acta Biochim. Biophys. Sin.* **2012**, *44*, 300−306.
(52) Trott, O.; Olson, A. J. AutoDock Vina: improving the speed and accuracy of docking with a new scoring function, efficient optimization, and multithreading. *J. Comput. Chem.* **2010**, *31*, 455−461.
(53) Pratt, W. B.; Toft, D. O. Steroid Receptor Interactions with Heat Shock Protein and Immunophilin Chaperones. *Endocr. Rev.* **1997**, *18*, 306−360.
(54) Ortiga-Carvalho, T. M.; Sidhaye, A. R.; Wondisford, F. E. Thyroid hormone receptors and resistance to thyroid hormone disorders. *Nat. Rev. Endocrinol.* **2014**, *10*, 582−591.
(55) Kirschke, E.; Goswami, D.; Southworth, D.; Griffin, P. R.; Agard, D. A. Glucocorticoid receptor function regulated by coordinated action of the Hsp90 and Hsp70 chaperone cycles. *Cell* **2014**, *157*, 1685−1697.
(56) Wang, L.; Zhang, J.; Bai, H.; Li, X.; Lv, P.; Guo, A. Specific detection of Vibrio parahaemolyticus by fluorescence quenching immunoassay based on quantum dots. *Appl. Biochem. Biotechnol.* **2014**, *173*, 1073−1082.
(57) Mittal, R.; Bruchez, M. P. Biotin-4-fluorescein based fluorescence quenching assay for determination of biotin binding capacity of streptavidin conjugated quantum dots. *Bioconjugate Chem.* **2011**, *22*, 362−368.
(58) Mortoglou, A.; Candiloros, H. The serum triiodothyronine to thyroxine (T3/T4) ratio in various thyroid disorders and after Levothyroxine replacement therapy. *Hormones* **2004**, *3*, 120−126.
(59) Chiha, M.; Samarasinghe, S.; Kabaker, A. S. Thyroid storm: an updated review. *J. Intensive Care Med.* **2015**, *30*, 131−140.
(60) Wallin, G.; Brönnegård, M.; Grimelius, L.; McGUIRE, J.; Tørring, O. Expression of the thyroid hormone receptor, the oncogenes c-myc and H-ras, and the 90 kD heat shock protein in normal, hyperplastic, and neoplastic human thyroid tissue. *Thyroid* **1992**, *2*, 307−313.
(61) Saibil, H. Chaperone machines for protein folding, unfolding and disaggregation. *Nat. Rev. Mol. Cell Biol.* **2013**, *14*, 630−642.
(62) Ng, L.; Kelley, M. W.; Forrest, D. Making sense with thyroid hormone–the role of T(3) in auditory development. *Nat. Rev. Endocrinol.* **2013**, *9*, 296−307.
(63) Miller, D. J.; Fort, P. E. Heat Shock Proteins Regulatory Role in Neurodevelopment. *Front. Neurosci.* **2018**, *12*, 821.
(64) Stepien, B. K.; Huttner, W. B. Transport, Metabolism, and Function of Thyroid Hormones in the Developing Mammalian Brain. *Front. Endocrinol.* **2019**, *10*, 209.
(65) Eng, L.; Lam, L. Thyroid Function During the Fetal and Neonatal Periods. *Neoreviews* **2020**, *21*, e30−e36.
(66) Farwell, A. P.; Dubord-Tomasetti, S. A.; Pietrzykowski, A. Z.; Leonard, J. L. Dynamic nongenomic actions of thyroid hormone in the developing rat brain. *Endocrinology* **2006**, *147*, 2567−2574.
(67) Leemans, M.; Couderq, S.; Demeneix, B.; Fini, J. B. Pesticides With Potential Thyroid Hormone-Disrupting Effects: A Review of Recent Data. *Front. Endocrinol.* **2019**, *10*, 743.
(68) Richter, C. P.; Münscher, A.; Santana Machado, D. S.; Wondisford, F. E.; Ortiga-Carvalho, T. M. Complete activation of thyroid hormone receptor β by T3 is essential for normal cochlear function and morphology in mice. *Cell. Physiol. Biochem.* **2011**, *28*, 997−1008.
(69) Gomaa, N. A.; Jimoh, Z.; Campbell, S.; Zenke, J. K.; Szczepek, A. J. Biomarkers for Inner Ear Disorders: Scoping Review on the Role of Biomarkers in Hearing and Balance Disorders. *Diagnostics* **2021**, *11*, 42.
(70) Heufelder, A. E.; Wenzel, B. E.; Gorman, C. A.; Bahn, R. S. Detection, cellular localization, and modulation of heat shock proteins in cultured fibroblasts from patients with extrathyroidal manifestations of Graves' disease. *J. Clin. Endocrinol. Metab.* **1991**, *73*, 739−745.
(71) Wu, J.; Liu, T.; Rios, Z.; Mei, Q.; Lin, X.; Cao, S. Heat Shock Proteins and Cancer. *Trends Pharmacol. Sci.* **2017**, *38*, 226−256.
(72) Watkins, R. A.; Evans-Molina, C.; Terrell, J. K.; Day, K. H.; Guindon, L.; Restrepo, I. A.; Mirmira, R. G.; Blum, J. S.; DiMeglio, L. A. Proinsulin and heat shock protein 90 as biomarkers of beta-cell stress in the early period after onset of type 1 diabetes. *Transl. Res.* **2016**, *168*, 96−106.e1.
(73) Castro, J. P.; Fernando, R.; Reeg, S.; Meinl, W.; Almeida, H.; Grune, T. Non-enzymatic cleavage of Hsp90 by oxidative stress leads to actin aggregate formation: A novel gain-of-function mechanism. *Redox Biol.* **2019**, *21*, 101108.
(74) Cho, K. F.; Ma, T. P.; Rose, C. M.; Kirkpatrick, D. S.; Yu, K.; Blake, R. A. Chaperone mediated detection of small molecule target binding in cells. *Nat. Commun.* **2020**, *11*, 465.
(75) López-Otín, C.; Kroemer, G. Hallmarks of Health. *Cell* **2021**, *184*, 33−63.
(76) Remaud, S.; GothiÃ, J. D.; Morvan-Dubois, G.; Demeneix, B. A. Thyroid hormone signaling and adult neurogenesis in mammals. *Front. Endocrinol.* **2014**, *5*, 62.
(77) Lee, J.; Rabbani, C. C.; Gao, H.; Steinhart, M. R.; Woodruff, B. M.; Pflum, Z. E.; Kim, A.; Heller, S.; Liu, Y.; Shipchandler, T. Z.; Koehler, K. R. Hair-bearing human skin generated entirely from pluripotent stem cells. *Nature* **2020**, *582*, 399−404.
(78) Mohammadi-Ostad-Kalayeh, S.; Hrupins, V.; Helmsen, S.; Ahlbrecht, A.; Stahl, F.; Scheper, T.; Preller, M.; Surup, F.; Stadler, M.; Kirschning, A.; Zeilinger, C. Development of a microarray-based assay for efficient testing of new HSP70/DnaK inhibitors. *Bioorg. Med. Chem.* **2017**, *25*, 6345−6352.
(79) Morris, G. M.; Huey, R.; Lindstrom, W.; Sanner, M. F.; Belew, R. K.; Goodsell, D. S.; Olson, A. J. AutoDock4 and AutoDockTools4: Automated docking with selective receptor flexibility. *J. Comput. Chem.* **2009**, *30*, 2785−2791.
(80) Jorgensen, W. L.; Chandrasekhar, J.; Madura, J. D.; Impey, R. W.; Klein, M. L. Comparison of simple potential functions for simulating liquid water. *J. Chem. Phys.* **1983**, *79*, 926−935.
(81) Phillips, J. C.; Braun, R.; Wang, W.; Gumbart, J.; Tajkhorshid, E.; Villa, E.; Chipot, C.; Skeel, R. D.; Kalé, L.; Schulten, K. Scalable molecular dynamics with NAMD. *J. Comput. Chem.* **2005**, *26*, 1781−1802.
(82) Best, R. B.; Zhu, X.; Shim, J.; Lopes, P. E.; Mittal, J.; Feig, M.; MacKerell, A. D., Jr. Optimization of the additive CHARMM all-atom protein force field targeting improved sampling of the backbone φ, ψ and side-chain $\chi(1)$ and $\chi(2)$ dihedral angles. *J. Chem. Theory Comput.* **2012**, *8*, 3257−3273.
(83) Huang, J.; Rauscher, S.; Nawrocki, G.; Ran, T.; Feig, M.; de Groot, B. L.; Grubmüller, H.; MacKerell, A. D., Jr. CHARMM36m: an improved force field for folded and intrinsically disordered proteins. *Nat. Methods* **2017**, *14*, 71−73.

https://doi.org/10.1021/acsomega.2c02331
ACS Omega 2022, 7, 28932−28945

(84) Vanommeslaeghe, K.; MacKerell, A. D., Jr. Automation of the CHARMM General Force Field (CGenFF) I: bond perception and atom typing. *J. Chem. Inf. Model.* **2012**, *52*, 3144−3154.
(85) Darden, T.; York, D.; Pedersen, L. Particle mesh Ewald: An N log (N) method for Ewald sums in large systems. *J. Chem. Phys.* **1993**, *98*, 10089−10092.
(86) Aqvist, J.; Marelius, J. The linear interaction energy method for predicting ligand binding free energies. *Comb. Chem. High Throughput Screening* **2001**, *4*, 613−626.

https://doi.org/10.1021/acsomega.2c02331
ACS Omega 2022, 7, 28932−28945